Mon. Not. R. Astron. Soc. **000**, 000–000 (0000) Printed 3 February 2008 (MN LATEX style file v2.2)

The Very Early Gamma-ray Burst Afterglows Powered by Structured Jets

T. Yan[1,2⋆], D. M. Wei[1,2] and Y. Z. Fan[1,2]
[1] *Purple Mountain Observatory, Chinese Academy of Sciences, Nanjing 210008, China*
[2] *National Astronomical Observatories, Chinese Academy of Sciences, Beijing, 100012, China*

Received... accepted...

ABSTRACT
If X-ray flashes (XRFs) and X-ray rich Gamma-ray Bursts(XRRGs) have the same origin with Gamma-ray Bursts (GRBs) but are viewed from larger angles of structured jets, their early afterglows may differ from those of GRBs. When the ultra-relativistic outflow interact with the surrounding medium, there are two shocks formed, one is a forward shock, the other is a reverse shock. In this paper we calculate numerically the early afterglow powered by uniform jet, Gaussian jet and power-law jet in the forward-reverse shock scenario. A set of differential equations are used to govern the dynamical evolution and synchrotron self-Compton effect has been taken into account to calculate the emission. In uniform jets, the very early afterglows of XRRGs and XRFs are significantly lower than GRBs and the observed peak times of RS emission are longer in interstellar medium environment. The RS components in XRRGs and XRFs are difficult to be detected. But in stellar wind, the reduce of very early flux and the delay of RS peak time are not so remarkable. In nonuniform jet(Gaussian jet and power-law jet), where there are emission materials on the line of sight, the very early light curve resembles isotropic-equivalent ejecta in general although the RS flux decay index shows notable deviation if the RS is relativistic(in stellar wind).

Key words: X-rays: general—Gamma-rays: bursts—radiation mechanism: non-thermal

1 INTRODUCTION

Late time Gamma-ray Burst (GRB) afterglow emission has been well observed and studied since the first detection in 1997(van Paradijs *et al.* 1997; Costa *et al.* 1997). In contrast, afterglow shortly after or during the main GRB is still quite uncertain because of the lack of observation. This early afterglow may provide important information about initial parameters of the burst and shed light on explosion mechanism. SWIFT is able to observe multi-wavelength radiation rapidly after γ ray triggering. With new observations, the early stage should be investigated more profoundly. In the standard baryonic GRB fireball model, prompt GRB emission is produced by collisions of internal shocks while afterglow comes from interactions between burst-ejected materials and circum-burst medium. After the internal shock phase, as the fireball is decelerated by the circumburst medium, usually a pair of shocks develop (Mészáros & Rees 1997; Sari & Piran 1999). One is a forward shock (FS) expands outward to heat the external medium, the other is a reverse shock (RS) propagates into the ejecta and heats this cold initial shell. The central energy is gradually transmitted to outer medium through shocked mediums and shocked ejecta. The early afterglow studied in this paper is during this transition stage.

Mészáros & Rees (1997) pointed out RS should emit detectable optical synchrotron photons. This prediction has been confirmed by the optical flash and the radio flare detected in GRB 990123(Akerlof *et al.* 1999; Kulkarni *et al.* 1999; Sari & Piran 1999; Mészáros & Rees 1999; Nakar & Piran 2004). The later more detailed investigation suggests that the RS region may be magnetized (Fan *et al.* 2002; Zhang, Kobayashi & Mészáros 2003; Panaitescu & Kumar 2004). The RS emission of GRBs in stellar wind medium has been discussed (Chevalier & Li 2000; Wu *et al.* 2003; Zou, Wu & Dai 2005). The RS emission powered by the magnetized outflow or neutron-fed outflow has been investigated in some detail (Fan, Wei & Wang 2004b; Zhang & Kobayashi 2005; Fan, Zhang & Wei 2005a). The pair-rich reverse shock emission has been discussed by Li et al. (2003a) and McMahon, Kumar & Piran (2005). Unfortunately, up to now, there are only a few additional candidates. They are GRB 021211 (Fox *et al.* 2003; Li et al. 2003b; Wei 2003; Kumar & Panaitescu 2003), GRB 041219a (Blake *et al.* 2005; Fan, Zhang & Wei 2005b) and GRB 050525a (Klotz *et al.* 2005; Shao & Dai 2005). Whether the lack of RS emission events is due to observational limits or theoretical problems may be settled by further observation.

⋆ E-mail: tyan@pmo.ac.cn

X-ray Flash (XRF) is an interesting phenomenon which resembles GRB. It is similar to GRB in many aspects except its lower peak energy (∼10keV) and lower isotropic energy (∼ 10^{51}ergs). Several models are proposed(Dermer, Chiang & Böttcher 1999; Heise *et al.* 2001; Huang, Dai & Lu 2002; Barraud *et al.* 2003; Lamb, Donaghy & Graziani 2005) among which the structured jet model is widely discussed. When a jet is ejected and propagating, observers on different viewing angles will see different phenomena. GRBs are observed near the jet center. XRFs may be detected at the edge of the jet. Between them are the X-ray rich GRBs (XRRGs) whose peak energies and isotropic energies are between those of GRBs and XRFs. Possible jet models for the XRFs and XRRGs include the off-beam uniform jet model (Ioka & Nakamura 2001; Yamazaki, Ioka & Nakamura 2002), the Gaussian jet model (Zhang & Mészáros 2002; Lloyd-Ronning, Dai & Zhang 2004; Zhang, Dai & Lloyd-Ronning 2004), and the power-law jet model(Mészáros *et al.* 1998; Jin & Wei 2004). The very early afterglow powered by structured jets has been calculated by Fan, Wei & Wang (2004a) analytically. In this work, we present our numerical results.

The dynamical evolution is described in Section 2. The radiation calculation procedure is shown in Section 3. Afterglows from jets are prsented in Section 4. In section 5, our results are summarized with some discussions.

2 DYNAMICAL EVOLUTION

Consider a homogenous cold shell ejected from central engine with isotropic energy E_{iso} and width Δ_0. It expands relativistically with Lorenz factor η and contains mass $m_{ej} = E_{iso}/\eta c^2$. When a FS and a RS are formed, there is a shocked region consists of tow parts: the shocked medium and the shocked shell separated by the contact discontinuity surface. The shocked region is assumed to have homogenous bulk velocity and energy density, that is, $\gamma_2 = \gamma_3$, $e_2 = e_3$ (hereafter the subscript 2 denotes the shocked medium, 3 denotes the shocked shell and 4 denotes the cold ejecta). However, the number density and random particle velocity in the comoving frame are discontinuous at the contact discontinuous surface. The random Lorentz factor of the shocked protons are $(\gamma_2 - 1) \approx \gamma_2$ and $(\gamma_{34} - 1)$ in regions 2 and 3, respectively (Blandford & Mckee 1976), where γ_{34} is the relative Lorentz factor of the shocked shell to the cold shell.

Kinetic energies of the shocked medium, the shocked shell and the unshocked shell are respectively:

$$\begin{aligned} E_2 &= (\gamma_2 - 1)m_2c^2 + (1-\epsilon_2)\gamma_2 U_2, \\ E_3 &= (\gamma_3 - 1)m_3c^2 + (1-\epsilon_3)\gamma_3 U_3, \\ E_4 &= (\eta - 1)(m_{ej} - m_3)c^2, \end{aligned}$$

where $U_2 = (\gamma_2 - 1)m_2c^2$ and $U_3 = (\gamma_{34} - 1)m_3c^2$ are internal energies in the comoving frame. If a fraction ϵ of the fresh shocked material energy is radiated, the radiated thermal energies of the shocked medium and shocked shell are $\epsilon_2\gamma_2(\gamma_2 - 1)dm_2c^2$ and $\epsilon_3\gamma_3(\gamma_{34} - 1)dm_3c^2$. With energy conservation, we have

$$\begin{aligned} d(E_2 + E_3 + E_4) = &-\epsilon_2\gamma_2(\gamma_2 - 1)dm_2c^2 \\ &-\epsilon_3\gamma_3(\gamma_{34} - 1)dm_3c^2. \end{aligned} \quad (1)$$

If GRBs are located in interstellar medium(ISM), the number density of the external medium n_1 is constant. If GRBs are born in stellar wind, $n_1 = AR^{-2}$, where $A = \dot{M}/4\pi m_p v_w = 3 \times 10^{35} A_* cm^{-1}$ and $A_* = (\dot{M}/1 \times 10^{-5} M_\odot yr^{-1}(v_w/10^3 km/s)^{-1}$(Chevalier & Li 2000). The swept-up mass of FS evolves as

$$\frac{dm_2}{dR} = 4\pi R^2 n_1 m_p. \quad (2)$$

The comoving number density of the ejecta $n_4 = M_{ej}/[4\pi m_p R^2 \Delta\eta]$, where $\Delta = max(\Delta_0, R/\eta^2)$ is the width of shell considering spreading effect. When R is smaller than the spreading radius $R_s = \Delta_0\eta^2$, $\Delta \approx \Delta_0$. If $R > R_s$, $\Delta \approx R/\eta^2$. The swept-up mass of RS evolves as

$$\frac{dm_3}{dR} = 4\pi R^2(\beta_4 - \beta_{RS})\eta\, n_4 m_p, \quad (3)$$

where $\beta_{RS} = \frac{\gamma_3 n_3 \beta_3 - \gamma_4 n_4 \beta_4}{\gamma_3 n_3 - \gamma_4 n_4}$, which is the Lorentz factor of RS (Fan, Wei & Wang 2004b). From equations (1-3), it is found that γ_2 evolves as

$$\frac{d\gamma_2}{dR} = -4\pi R^2 \frac{Q}{P}, \quad (4)$$

where

$$\begin{aligned} Q &= (\gamma_2^2 - 1)n_1 m_p + (\gamma_2\gamma_{34} - \eta)(\eta n_4 m_p)(\beta_4 - \beta_{RS}), \\ P &= m_2 + m_3 + (1-\epsilon_2)(2\gamma_2 - 1)m_2 + (1-\epsilon_3)(\gamma_{34} - 1)m_3 \\ &\quad +(1-\epsilon_3)\gamma_2 m_3[\eta(1 - \beta_2\beta_4) - \frac{\eta\beta_4}{\gamma_2^2\beta_2}]. \end{aligned}$$

The overall dynamical evolution of RS-FS can be obtained by solving equations (2-4) combined with

$$dR = \frac{\beta_2}{1-\beta_2}\frac{cdt}{1+z} \quad (5)$$

where t is the time measured by the observer and z is the redshift.

Define η_e to be the electron radiative efficiency, that is, a fraction η_e of the electron energy is radiated. In the fast cooling stage, electrons cool immediately and $\eta_e = 1$. In the slow cooling stage, $\eta_e = (\gamma_m/\gamma_c)^{p-2}$ (Sari & Esin 2001), where γ_m and γ_c are the minimum and the cooling Lorentz factor of the shocked electrons, respectively (see detail in the next section). Usually it is assumed that electrons share a fraction ϵ_e of internal energy. Then the radiative efficiency is

$$\epsilon = \epsilon_e\eta_e = \epsilon_e \min[1, (\gamma_m/\gamma_c)^{p-2}]. \quad (6)$$

$\epsilon = 0$ corresponds to the adiabatic case while $\epsilon = 1$ corresponds to the fully radiative case.

Sari & Piran (1995) introduced $\xi \equiv (l/\Delta_0)^{1/2}\eta^{-4/3}$ to describe the strength of the RS, where $l \equiv [3E_{iso}/(4\pi n_1 m_p c^2)]^{1/3}$ is the Sedov length. If $\xi < 1$ at the RS crossing time ($t_\times$), the RS is relativistic (RRS). If $\xi > 1$ at $t_\times$, the RS is non-relativistic (NRS). Our results are consist with them. The scaling laws are exactly the same with analytical results though differences exist in absolute values. In our numerical results, it is found out that $\gamma_{34} - 1$ can be well fitted by

$$\begin{aligned} \lg(\gamma_{34} - 1) = &-0.64991 - 1.64406\lg\xi \\ &-0.59494(\lg\xi)^2 - 0.13656(\lg\xi)^3. \end{aligned} \quad (7)$$

for $0.01 < \xi < 10$.

After the RS crosses the shell, the shocked medium and the shocked ejecta evolve somewhat independently. The FS continues to spread outwards, collect external medium and the

shocked medium is gradually shaped into BM self-similar profile. The energy conservation still applies:

$$dE_2 = -\epsilon_2\gamma_2(\gamma_2-1)dm_2c^2 \qquad (t > t_\times). \tag{8}$$

Then the forward shock evolution can be solved together with equation(2), (5) and (8). At the same time, the shocked ejecta ceases to increase, *i.e.*, $m_3 = m_{ej} = const$ for $t > t_\times$. Koboyashi & Sari (2000) showed that its evolution consists approximately with BM solution, that is, $\gamma_3 \propto R^{-7/2+k}(k = 0$ applies to ISM and $k = 2$ to wind). They also inferred that the shocked ejecta spreads with the speed of light in the comoving frame and evolves adiabatically.

3 RADIATION

Both FS and RS heat the cold materials to higher temperatures, accelerate protons and electrons as well as generate random magnetic field. Here we calculate the synchrotron radiation and the synchrotron self-Compton cooling of the shocked electrons. The internal energy density of FS shocked medium $e_2 = 4\gamma_2^2 n_1 m_p c^2$(Blandford & Mckee 1976). For the ejecta shocked by RS, $e_3 = e_2$ before $t_\times$, otherwise $e_3 \propto t^{-\frac{4(3+g)}{3(1+2g)}}(g = 7/2-k)$. ϵ_e and ϵ_B are defined to be the faction of internal energy occupied by electrons and magnetic field. It is easy to get that magnetic field $B = \sqrt{8\pi\epsilon_B e}$. As to electrons, in the absence of energy loss, they are assumed to be shocked to a power-law distribution $dN_e/d\gamma_e \propto \gamma_e^{-p}(\gamma_m < \gamma_e < \gamma_M)$ with minimum Lorentz factor

$$\gamma_{m,2} = \epsilon_e(\gamma_2-1)\frac{m_p(p-2)}{m_e(p-1)} + 1,$$

$$\gamma_{m,3} = \epsilon_e(\gamma_{34}-1)\frac{m_p(p-2)}{m_e(p-1)} + 1,$$

and maximum Lorentz factor $\gamma_M = 10^8(B/1G)^{-1/2}$(Dai & Lu 2001). Here e and B are all measured in the coming frame. Following Sari *et al.* (1998), we introduce the cooling Lorentz factor $\gamma_c = \frac{6\pi(1+z)m_e c}{\sigma_T\gamma B^2 t}$ to describe the synchrotron radiation loss of the shocked electrons. Note that $\gamma_{c,3} = \gamma_{c,2}$ before $t_\times$. The actual electron distribution should be given as following (see also Fan, Wei & Wang (2004b)): (i) for $\gamma_c \leqslant \gamma_m$, i.e., the fast cooling case

$$\frac{dN_e}{d\gamma_e} = C_1\begin{cases}\gamma_e^{-2}, & (\gamma_c \leqslant \gamma_e \leqslant \gamma_m),\\ \gamma_m^{p-1}\gamma_e^{-(p+1)}, & (\gamma_m < \gamma_e \leqslant \gamma_M),\end{cases} \tag{9}$$

where

$$C_1 = [\frac{1}{\gamma_c} - \frac{p-1}{p}\frac{1}{\gamma_m} - \frac{\gamma_m^{p-1}\gamma_M^{-p}}{p}]^{-1}N_{\rm tot}\,,$$

where $N_{\rm tot}$ is the total number of radiating electrons involved; (ii) for $\gamma_m < \gamma_c \leqslant \gamma_M$, i.e., the slow cooling case

$$\frac{dN_e'}{d\gamma_e} = C_2\begin{cases}\gamma_e^{-p}, & (\gamma_m \leqslant \gamma_e \leqslant \gamma_c),\\ \gamma_c\gamma_e^{-(p+1)}, & (\gamma_c < \gamma_e \leqslant \gamma_M),\end{cases} \tag{10}$$

where

$$C_2 = [\frac{\gamma_m^{1-p}}{p-1} - \frac{\gamma_c^{1-p}}{p(p-1)} - \frac{\gamma_c\gamma_M^{-p}}{p}]^{-1}N_{\rm tot}.$$

In the comoving frame, the synchrotron radiation of the two-segment distributed electrons can be well described by power-law spectrum consisted of several segments. The spectrum peaks at $\min(\nu_m', \nu_c')$ with flux(Wijers & Galama 1999)

$$F'_{max} = \Phi_p\frac{\sqrt{3}e^3 B N_{\rm tot}}{m_e c^2}, \tag{11}$$

where Φ_p is a function of p(for $p \simeq 2.5, \Phi_p \simeq 0.60$). The breaking frequencies corresponding to γ_m and γ_c are $\nu_m' = 3\gamma_m^2 eB/(4\pi m_e c)$ and $\nu_c' = 3\gamma_c^2 eB/(4\pi m_e c)$. The absorption frequency ν_a', under which the synchrotron self-absorption can not be ignored, is calculated accordingly Wu *et al.* (2003). These three breaking frequencies divide the spectrum into four segments. The spectrum indices are, from low frequency to high frequency, (i)for $\nu_a' < \nu_m' < \nu_c'$, $[2, 1/3, (1-p)/2, -p/2]$; (ii)for $\nu_a' < \nu_c' < \nu_m'$, $[2, 1/3, -1/2, -p/2]$; (iii)for $\nu_m' < \nu_a' < \nu_c'$, $[2, 5/2, (1-p)/2, -p/2]$; (iv)for $\nu_c' < \nu_a' < \nu_m'$, $[2, 5/2, -1/2, -p/2]$; (v)for $\nu_m' < \nu_c' < \nu_a'$ and $\nu_c' < \nu_m' < \nu_a'$, $[2, 5/2, 5/2, -p/2]$.

We assume that the synchrotron power is radiated isotropically in the comoving frame, $\frac{dF'(\nu')}{d\Omega'} = \frac{F'(\nu')}{4\pi}$. The angular distribution of power in the observer's frame is(Rybicki & Lightman 1976; Huang *et al.* 2000)

$$\frac{dF(\nu)}{d\Omega} = \frac{1+z}{\gamma^3(1-\beta\mu)^3}\frac{dF'(\nu')}{d\Omega'} = \frac{1+z}{\gamma^3(1-\beta\mu)^3}\frac{F'(\nu')}{4\pi}, \tag{12}$$

where

$$\nu = \frac{\nu'}{(1+z)\gamma(1-\mu\beta)}. \tag{13}$$

Then the observed flux density at frequency ν is

$$\begin{aligned} S_\nu &= \frac{1}{A}\left(\frac{dF(\nu)}{d\Omega}\frac{A}{D_{\rm L}^2}\right)\\ &= \frac{1+z}{\gamma^3(1-\beta\mu)^3}\frac{1}{4\pi D_{\rm L}^2}F'\left((1+z)\gamma(1-\mu\beta)\nu\right), \end{aligned} \tag{14}$$

where A is the area of our detector and $D_{\rm L}$ is the luminosity distance (we assume $H_0 = 65$km s^{-1} Mpc^{-1}, $\Omega_M = 0.3$, $\Omega_\wedge = 0.7$).

After the RS crosses the shell, no new electrons are accelerated in the shocked shell anymore and all the electrons cool at the same rate caused by the adiabatic expansion of the fluid. No electrons exist above γ_c, so the flux above ν_c' drops exponentially.

At a particular time t, the photons received by the observer comes from an equal arriving time surface determined by (Huang *et al.* 2000)

$$t = (1+z)\int\frac{1-\beta\cos\Theta}{\beta c}dR \equiv \text{const.}, \tag{15}$$

where Θ is the angle between the radiation region and the viewing line in the burst frame.

We also consider synchrotron self-Compton (SSC) effect. It will reduce the cooling Lorentz factor to

$$\gamma_c = \frac{\gamma_c^{syn}}{1+Y}, \tag{16}$$

where Y is the Compton parameter, expressed as (Sari & Esin 2001; Wang, Dai & Lu 2001)

$$Y = \frac{L_{ICS}}{L_{syn}} = \frac{\eta_e\epsilon_e/\epsilon_B}{1+Y} = \frac{-1+\sqrt{1+4\eta_e\epsilon_e/\epsilon_B}}{2}. \tag{17}$$

Take it into equation(16), γ_c can be solved numerically. At early time, the forward shocked material is in the fast cooling phase and the cooling frequency will be reduced significantly due to the SSC radiation. As to the RS, whether it is in the fast or slow cooling phase is parameters dependent. However, even if it is in

slow cooling phase, the cooling frequency will be suppressed by SSC if $\epsilon_e/\epsilon_B \gg 1$, which is the ordinary case.

4 NUMERICAL RESULTS

In this section the early afterglow from isotropic ejecta is presented at first. Then we calculate afterglows powered by different jets. Three kinds of jets are considered. They are the uniform jet, the Gaussian jet, and the power-law jet. The sideways expansion of these jets is ignored in our calculation.

The obstacle we encountered in the current work is the poorly known initial Lorentz factor of these jets, especially for the structured ones (The Gaussian jet and power-law jet). By now, the spectrum of most XRFs are non-thermal. The emitting region should be optical thin, i.e., the optical thickness $\tau = n_{\rm e}\sigma_{\rm T}R' < 1$, where R' is the comoving width of the emitting region, $n_{\rm e} \approx \frac{L}{16\pi\epsilon_{\rm e}\eta^5 m_{\rm p}c^4\delta t R'}$ is the comoving number density of electrons contained in the emitting region. L is the isotropic luminosity of the burst, δt is the typical variability timescale of the burst lightcurve. Assuming that XRFs are powered by internal shocks, the optical thin ($\tau < 1$) condition yields (e.g., Fan & Wei (2005))

$$\eta \geqslant 30 L_{49}^{1/5}\delta t_{-2}^{-1/5}. \quad (18)$$

Kumar & Granot (2003) have performed a numerical investigation on the hydrodynamical evolution of a Gaussian jet by assuming $\eta(\theta)$ is also Gaussian. In the Monte Carlo simulation of Zhang et al. (2004), $\eta(\theta)$ has been taken as a free function but to find that a flat or only small fluctuation angular distribution of Lorentz factor is indeed required. Therefore, and partly for convenience, we take $\eta = 300$ for off-axis uniform jet, the Gaussian jet, and the power-law jet.

For each jet model, light curves with typical parameters from three viewing angles are presented, which may correspond to GRBs, XRRGs and XRFs respectively. The light curves differ from each other although there are some universal properties. Viewing from the center of a jet, the light curve is approximately the same as that powered by an isotropic ejecta at the early time and a break occurs when the emission from the edge comes into view. When we observe off-axis, the flux is lower at the early time but gradually converge into the light curve from the center when the whole jet can be seen.

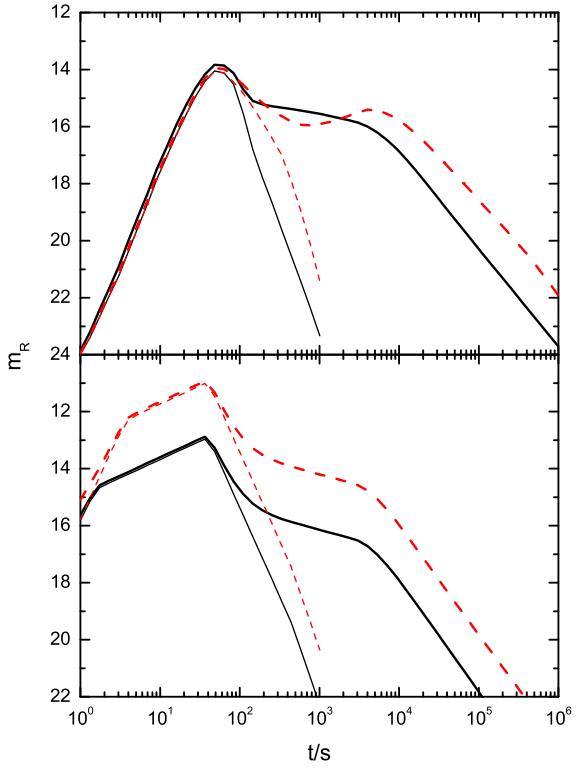

Figure 1. R band afterglow from isotropic ejecta with typical parameters. Upper panel is the ISM case and lower is the wind case. Thin lines are the RS emission and thick lines are the total emission. SSC effect is ignored in the dashed lines and taken into account in the solid lines. In the ISM case, the shape of the light curve changed since $\nu_c^{RS}, \nu_c^{FS} \sim \nu_R$ around $t_\times$. The RS shows a more rapid decay and the bump caused by the FS vanishes. In the wind case, both RS and FS flux are reduced since $\max(\nu_c^{RS}, \nu_c^{FS}) < \nu_R$. Parameters: $\eta = 300$, $\Delta_0 = 3 \times 10^{11} cm$, $E_{iso} = 1 \times 10^{53} ergs$, $n_1 = 1 cm^{-3}$ for ISM and $\eta = 300$, $\Delta_0 = 1 \times 10^{12} cm$, $E_{iso} = 5 \times 10^{52} ergs$, $A_* = 1.0$ for wind, $\epsilon_e = 0.3, \epsilon_B = 0.01, p = 2.5, z = 1$.

4.1 Isotropic ejecta

The upper panel of Fig.1 shows the early R band light curve from isotropic ejecta in ISM case with typical parameters. The RS dominates the very early R band light curve, peaks at about 14mag. The RS is non-relativistic at $t_\times$ with $\nu_m^{RS} < \nu_a^{RS} < \nu_R < \nu_c^{RS}$. Therefore $t_\times \approx 45s$ is greater than the prompt duration $T_{dur} = (1+z)\frac{\Delta_0}{c} \approx 20s$. The R band arising index is ~ 2.5, which is shallower than the analytical estimation of NRS (Koboyashi 2000; Fan *et al.* 2002). It varies with time as well as with initial parameters (Nakar & Piran 2004). After $t_\times$, the decay index is ~ 2 until $\nu_c^{RS} = \nu_R$. Then a break occurs followed by faster decay. The flux after the break comes from equal arriving time surface emitted at lower radius. Since ν_c is reduced by SSC, it reaches the R band and the RS flux encounters faster decay shortly after $t_\times$. Due to the rapid decay of RS emission, the later emission is mainly contributed by FS. It is interesting to note that the late FS emission bump vanishes when the SSC effect has been taken into account. The physical reason is that with SSC effect, the FS flux peak time appears earlier at $\nu_R = \nu_c^{FS}$ during fast cooling. Since $\nu_c^{FS} \propto t^{-1/2}, \nu_m^{FS} \propto t^{-3/2}$ and $F_{max}^{FS} \sim const$, the decay index following the peak flux is quite flat(-1/4) and change to $-(3p-2)/4$ after $\nu_R = \nu_m^{FS}$.

In stellar wind environment, the RS also dominates the very early R band light curve with typical parameters, which is shown in the lower panel of Fig.1. The peak flux is about 13mag. The RS is relativistic at $t_\times$ with $\nu_c^{RS} < \nu_a^{RS} < \nu_R < \nu_m^{RS}$. $t_\times \approx 40s$ coincides with $T_{dur} \approx 65s$. The R band arising index is ~ 0.5, which is much flatter than that in the ISM case. After $t_\times$, the flux decay with -2.5, which is contributed to emission from lower radius on equal arrival time surface. Since both RS and FS are in the fast cooling case and $\max\{\nu_c^{RS}, \nu_c^{FS}\} < \nu_R$, the R band flux is reduced by a factor $1+Y \simeq 1+\sqrt{\epsilon_e/\epsilon_B}$(about 2 magnitude taking $\epsilon_e/\epsilon_B = 30$) when the SSC effect has been taken into account.

4.2 Uniform jet

Uniform jet is a simple model which assumes that all the ejected materials are confined to a collimated uniform cone. GRBs are detected within the cone (on-beam). XRFs and XRRGs are viewed out of the jet(off beam). If our viewing angle Θ_v is slightly larger than the jet opening angle θ_{jet}, the observed frequency

$$\nu_{off} = a\nu_{on}, \tag{19}$$

where $a \approx [1+\gamma^2(\Delta\Theta)^2]^{-1}$ (γ is the bulk Lorentz factor of the jet) and $\Delta\Theta = \Theta_v - \theta_{jet}$. Taking the peak energy of XRFs $E_{p,XRF} \approx 0.1E_{p,GRB}$, XRFs should be observed at $\Delta\Theta_{XRF} \approx 3/\eta$. The observed flux can be estimated by an empirical formula (e.g., Fan, Wei & Wang (2004a))

$$F_{\nu_{off}}(\Delta\Theta, t_{obs}) \approx \frac{a^3}{2} F_{\nu_{on}}(0,t), \tag{20}$$

where $dt_{obs} = dt/a$. It implies that if $\gamma > 1/\Delta\Theta$,the observed flux is dramatically lower and the observed time is longer. The early afterglow powered by the uniform jets has been presented in Fig. 2.

In the ISM case, the flux increases rapidly at the early time. The RS component reaches its peak flux at a time longer than viewing on-beam. The peak flux of RS emission for $\Delta\Theta = 3/(2\eta)$ (i.e., the XRRG) is about 17.5mag at about 100s. It is bright enough to be detected. The rising index of RS is about 3.5. The peak flux of the RS emission for $\Delta\Theta = 3/\eta$ (i.e., the XRF) is about 21mag at about 250s. It is hard to be detected by UVOT on SWIFT or ground telescope at such early time. The rising index is about 4.2. After $t_\times$, the observed FS flux keeps rising for some while, peaks several hours later. The peak FS emission flux of XRRG is about 17mag and 17.5mag for XRF. Therefore in XRFs, the RS component can hardly be seen and the later FS component around 1hour is much more luminous. In XRRG, the RS emission is detectable but the RS component is not significant. The light curve is nearly flat for t <1 hour.

In the wind case, the off-beam RS very early flux increases at the same rate as in the on-beam case since both γ and a are constant, but the flux is lower. The peak time of off-beam RS is slightly longer, $\sim 50s$ in XRF. The XRF peak flux is about 15mag and significantly higher than the FS. After $t_\times$, as the Lorentz factor decreases, the light curve gradually converge into the light curve from the center.

4.3 Nonuniform jet

Different from uniform jets, there are emission materials on the line of sight in nonuniform jets(Gaussian jets and power-law jets). XRFs and XRRGs are viewed within the jets but have lower isotropic-equivalent energy than GRBs. The observed early emission is mainly contributed from materials on the line of sight. However, we find that the light curve show notable deviation if the RS is relativistic.

4.3.1 Gaussian jet

The jet energy in a Gaussian jet distributed with angular as

$$E(\theta) = E_0 e^{-\theta^2/2\theta_0^2} \qquad 0 \leqslant \theta \leqslant \theta_{jet}. \tag{21}$$

With typical value that $E_{iso,XRF} = 10^{-2}E_{iso,GRB}$, the viewing angle of XRF should be $\Theta_{v,XRF} \approx 3.04\theta_0$. We also calculate the light curve with $\Theta_{v,XRRG} \approx 2.15\theta_0$ which may correspond to the XRRG(taking $E_{iso,XRRG} = 10^{-1}E_{iso,GRB}$). The R band afterglow from Gaussian jet is shown in Fig.3.

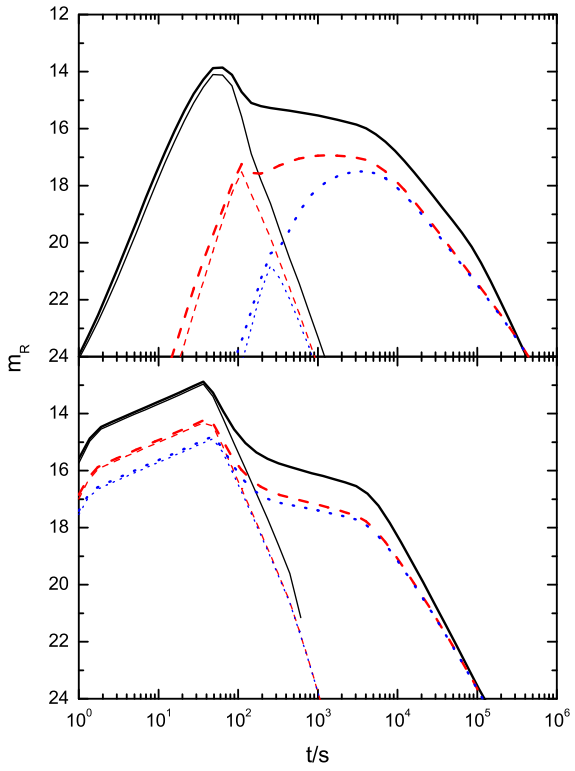

Figure 2. R band afterglow from uniform jet. Upper panel is the ISM case and lower is the wind case. Thin lines are the RS emission and thick lines are the total emission. $\Delta\Theta = 0,\ 3/2\eta,\ 3/\eta$ in solid lines, dashed lines and dotted lines respectively. Parameters: $\theta_{jet} = 0.1$, other parameters are the same as in Fig.1.

In the ISM case, the off-axis RS flux is exactly the same with isotropic emission taking $E_{iso} = E(\Theta_v)$. The RS is non-relativistic and the Lorentz factor is high at early time. So the jet structure can not change the light curve significantly. As Θ_v increases, the light curve has (i) shorter $t_\times$; (ii)lower peak RS emission flux, about 17mag for XRRG and 19.5mag for XRF; (iii) flatter rising before $t_\times$; (iv) longer t_{Rc}(the time $\nu_R = \nu_c$), therefore longer time interval for the ~ -2 delay after $t_\times$.

In stellar wind, the off-axis RS flux is slightly different with the isotropic emission taking $E_{iso} = E(\Theta_v)$. The RS is relativistic and the Lorentz factor is sufficiently low to reflect the jet structure. The isotropic emission with decreasing E_{iso} from GRB to XRF has (i)nearly constant $t_\times$, constant rising index 0.5 before $t_\times$ and decay index -2.5 after $t_\times$; (ii)lower peak flux, about 16.5mag for XRRG and 19mag for XRF. What actual light curve differs from isotropic one is the decay index of RS flux. Viewing from the center, RS flux decays faster. With increasing viewing angle, the start time of the faster decay increases, and from $t_\times$ to this time, the flux is flatter than isotropic emission. The surplus emission comes from the center of the jet with $\theta < \Theta_v$.

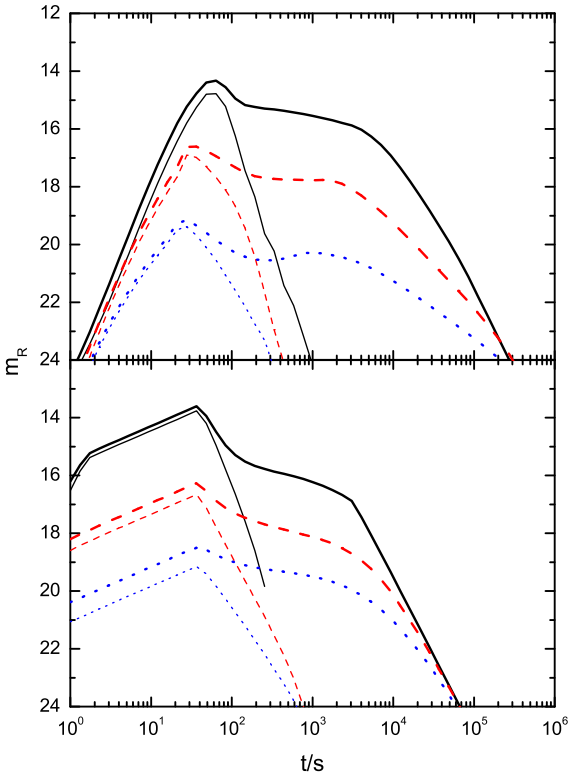

Figure 3. R band afterglow from Gaussian jet. Upper panel is the ISM case and lower is the wind case. Thin lines are the RS emission and thick lines are the total emission. $\Theta_v = 0, 2.15\theta_0, 3.04\theta_0$ in solid lines, dashed lines and dotted lines respectively. Parameters: $E_0 = 1\times10^{53} ergs$ for ISM and $E_0 = 5\times10^{52} ergs$ for wind, $\theta_0 = 0.05$,$\theta_{jet} = 0.2$, other parameters are the same as in Fig.1.

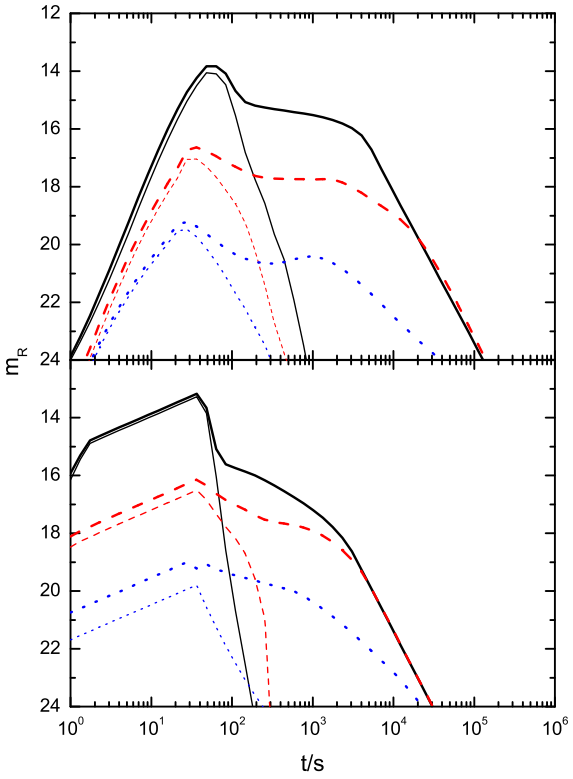

Figure 4. R band afterglow from power-law jet. Upper panel is the ISM case and lower is the wind case. Thin lines are the RS emission and thick lines are the total emission. $\Theta_v = 0, 3.16\theta_c, 10\theta_c$ in solid lines, dashed lines and dotted lines respectively. Parameters: $E_c = 1 \times 10^{53} ergs$ for ISM and $E_c = 5 \times 10^{52} ergs$ for wind, $\theta_c = 0.015$, $\theta_{jet} = 0.2$, other parameters are the same as in Fig.1.

4.3.2 Power-law jet

In this model, the jet energy distribution as a function of angular is as follows

$$E(\theta) = \begin{cases} E_c & 0 \leqslant \theta < \theta_c \\ E_c(\theta/\theta_c)^{-2} & \theta_c \leqslant \theta \leqslant \theta_{jet}. \end{cases} \quad (22)$$

$E_{iso,XRF} = 10^{-2} E_{iso,GRB}$ and $E_{iso,XRRG} = 10^{-1} E_{iso,GRB}$ correspond to $\Theta_{v,XRF} \approx 10\theta_c$ and $\Theta_{v,XRRG} \approx 3.16\theta_c$ respectively. Early afterglow from power-law jet is shown in Fig.4.

In the ISM case, the RS is also exactly the same with isotropic emission taking $E_{iso} = E(\Theta_v)$, as found in the Gaussian jet model. In the wind case, RS flux also resembles that in the Gaussian jet except the decay index departure from isotropic emission is more prominent.

5 CONCLUSION AND DISCUSSION

So far, there are several RS emission candidates reported in SWIFT era. One is GRB 041219a detected by INTEGRAL. Fan, Zhang & Wei (2005b) fitted its early IR afterglow with RS-FS emission model and found the RS region is magnetized. GRB 050525a may also be an possible candidate. Shao & Dai (2005) used RS-FS in standard scenario to fit the early optical bump and the parameters are reasonable.

However, among all the bursts targeted in optical band within few minutes after the prompt emission, only a small fraction of them have likely RS emission. This is conflicted with the theoretical estimation. It may be caused by the extinctions of the host galaxy. And as demonstrated in this paper, the overestimation of the ν_m, ν_c may lead to a dimmer RS radiation. Up to now, the very early optical afterglows of XRFs have not been well detected, future observation may help us to modify the present theory.

In this paper, we calculate the early afterglow powered by various kinds of jets numerically. Dynamical evolution is solved from a set of differential equations. This is different from the analytical treatment of Fan, Wei & Wang (2004a) and gives similar but more exactly results. We find that the most unprecise estimation comes from $\gamma_{34} - 1$, which results in the overestimation of ν_m and too rapid increasement of ν_m before $t_\times$ in previous treatment. This is especially significant in the ISM case since the RS is mildly relativistic in typical parameters taken here. At the same time, ν_c was overestimated previously because of the ignoring of SSC effect. Considering these two factors, the peak flux of reverse shock should be dimmer, which may help us to explain the lack of detection of optical flashes in most GRBs. It also needs to be pointed out that electrons may be cooled not only by SSC process but also by external photons(*e.g.*, prompt emission) through inverse Compton scattering. Then ν_c may

be reduced further and lead to even fainter very early optical radiation.

Early afterglow from jets, both uniform and structured, are calculated. We find that the early afterglow varies significantly with different viewing angles and is dependent on the jet structure.

SWIFT XRT detection find that the early X-ray flare may be an common characteristic of GRB X-ray afterglow. Fan & Wei (2005) suggested that the RS synchrotron emission hardly can produce the very early X-ray flares. Our calculation confirms their results. We also tried to simulate it with RS SSC emission within a large parameters space but failed. The RS SSC X-ray emission is always lower and generally far lower than FS synchrotron emission.

ACKNOWLEDGMENTS

We thank Zou, Y. C. and Jin, Z. P. for helpful discussion. This work is supported by the National Natural Science Foundation (grants 10225314 and 10233010) of China, and the National 973 Project on Fundamental Researches of China (NKBRSF G19990754).

REFERENCES

Akerlof, C. W., *et al.* 1999, *nature*, 398, 400
Barraud, C. *et al.* 2003, *A&A*, 400, 1021
Blake, C. H., *et al.* 2005, *nature*, 435, 181
Blandford, R. D. & Mckee, C. F. 1976, *Phys. Fluids*, 19, 1130
Chevalier, R. A. & Li, Z. Y. 2000, *ApJ*, 536, 195
Costa, E. *et al.* 1997, *nature*, 387,783
Dai, Z. G. & Lu, T. 2001, *ApJ*, 551, 249
Dermer, C. D., Chiang J., & Böttcher, M. 1999, *ApJ*, 513, 656
Fan, Y. Z., Dai, Z. G., Huang, Y. F. & Lu, T. 2002, *ChJAA*, 2, 449
Fan, Y. Z. & Wei, D. M. 2005, *MNRAS* Letters, in press (astro-ph/0506155)
Fan, Y. Z., Wei, D. M. & Wang, C. F. 2004a, *MNRAS* , 351, L78
Fan, Y. Z., Wei, D. M. & Wang, C. F. 2004b, *A&A*, 424, 477
Fan, Y. Z., Zhang, B. & Wei, D. M. 2005a, *ApJ*, 628,298
Fan, Y. Z., Zhang, B. & Wei, D. M. 2005b, *ApJ*, 628,L25
Fox, D. W., *et al.* 2003, *ApJ*, 586, L5
Heise, J., in't Zand, J., Kippen, R. M., & Woods, P. M. 2001, in Proc. of the conference "Gamma-ray Bursts in the Afterglow Era", 16
Huang, Y. F., Dai, Z. G. & Lu, T. 2002, *MNRAS*, 332, 735
Huang, Y. F., Gou, L. J., Dai, Z. G. & Lu, T. 2000, *ApJ*, 543, 90
Ioka, K. & Nakamura, T. 2001, *ApJ*, 554, L163
Jin, Z. P. & Wei, D. M. 2004, *ChJAA*, 4, 473
Klotz, A., Boer, M., Atteia, J. L., Stratta, G., Behrend, R., Malacrino, F. & Damerdji Y. 2005, *A&A*, 439, L35
Koboyashi, S. & Sari, R. 2000, *ApJ*, 542, 819
Koboyashi, S. 2000, *ApJ*, 545, 807
Kumar, P. & Panaitescu, A 2003, *MNRAS* , 346, 905
Kumar, P. & Granot, J. 2003, *ApJ*, 591, 1075
Kulkarni, S. R. 1999, *ApJ*, 522, L97
Lamb, D. Q., Donaghy, T. Q. & Graziani, C. 2005, *ApJ*, 620, L355
Li, Z., Dai, Z. G., Lu, T., & Song, L. M. 2003, *ApJ*, 599, 380
Li, W., Filippenko, A. V., Chornock, R., & Jha, S. 2003, *ApJ*, 586, L9
Lloyd-Ronning, N. M., Dai, X. Y. & Zhang, B. 2004, *ApJ*, 601, 371
McMahon, E., Kumar, P., & Piran, T. 2005, *MNRAS* , submitted (astro-ph/0508087)
Mészáros, P. & Rees, M. J. 1997, *ApJ*, 476,332
Mészáros, P., Rees, M. J., Wijers, R. A. M. J. 1998, *ApJ*, 499, 301
Mészáros, P. & Rees, M. J. 1999, *MNRAS* , 306, L39
Nakar, E. & Piran, T. 2004, *MNRAS* , 353, 647
Panaitescu, A. & Kumar, P. 2004, *MNRAS* , 353, 511
Rybicki, G. B. & Lightman, A. P. 1979, Radiative Processes in Astrophysics (New York: Wiley)
Sari, R., Piran, T. & Narayan, R. 1998, *ApJ*, 497, L17
Sari, R. & Piran, T. 1995, *ApJ*, 455, L143
Sari, R. & Piran, T. 1999, *ApJ*, 517, L109
Sari, R. & Esin, A. A. 2001, *ApJ*, 548, 787
Shao, L. & Dai, Z. G. 2005, *ApJ*, in press(astro-ph/0506139)
van Paradijs, J. *et al.* 1997, *nature*, 386,686
Wang, X. Y., Dai, Z. G. & Lu, T. 2001, *ApJ*, 546, L33
Wei, D. M. 2003, *A&A*, 402, L9
Wijers, R. A. M. J. & Galama, T. J. 1999, *ApJ*, 523, 177
Wu, X. F., Dai, Z. G., Huang, Y. F. & Lu, T. 2003, *MNRAS* , 342, 1131
Yamazaki, R., Ioka, K. & Nakamura, T. 2002, *ApJ*, 572, L31
Zhang, B., & Kobayashi, S. 2005, *ApJ*, 628, 315
Zhang, B. & Mészáros, P. 2002, *ApJ*, 571, 876
Zhang, B., Kobayashi, S. & Mészáros, P. 2003, *ApJ*, 595, 950
Zhang, B., Dai, X. Y., Lloyd-Ronning, N. M., Mészáros, P. & 2004, *ApJ*, 601, L119
Zou, Y. C., Wu, X. F. & Dai, Z. G. 2005, *MNRAS*, in press(astro-ph/0508602)